Electronic Supplementary Material (ESI) for Organic & Biomolecular Chemistry.

Synthesis of new fluorescent bichromophoric compounds as ratiometric pH probes for intracellular measurements

A. Vanessa Saura,[1] María J. Marín,[2] M. Isabel Burguete,[1] David A. Russell,[2]
Francisco Galindo,*[,1] Santiago V. Luis*[,1]

E-mail: francisco.galindo@uji.es, luiss@uji.es

[1] Departamento de Química Inorgánica y Orgánica, Universitat Jaume I, Av. Sos Baynat s/n, E-12071 Castellón (Spain)

[2] School of Chemistry, University of East Anglia, Norwich Research Park, Norwich, Norfolk, NR4 7TJ (UK)

Supporting Information

Spectroscopic characterization of the compounds

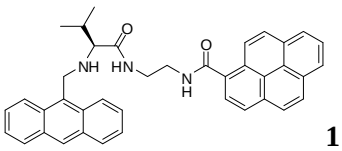

1

a

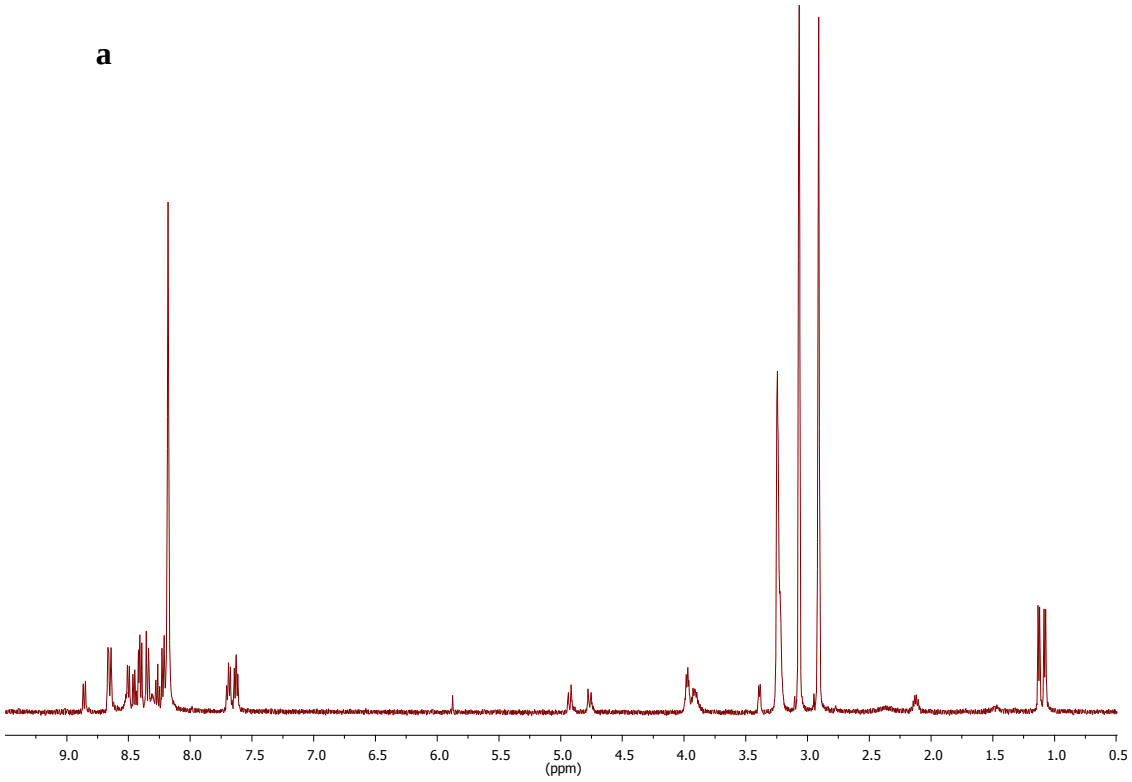

The ^{13}C-NMR spectrum of compound **1** could not be registered due to the limited solubility of this compound in the most common deuterated solvents.

b

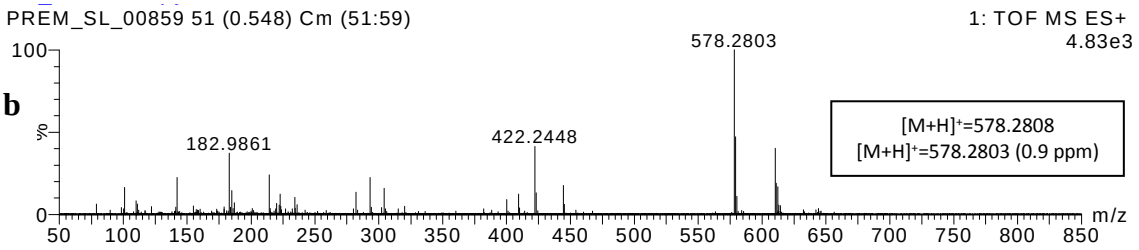

Fig. S1. a) ^{1}H-NMR spectrum in DMF-d_7 and **b)** ESI-TOF spectrum of compound **1**.

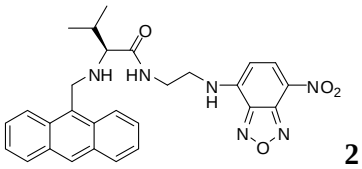

2

a

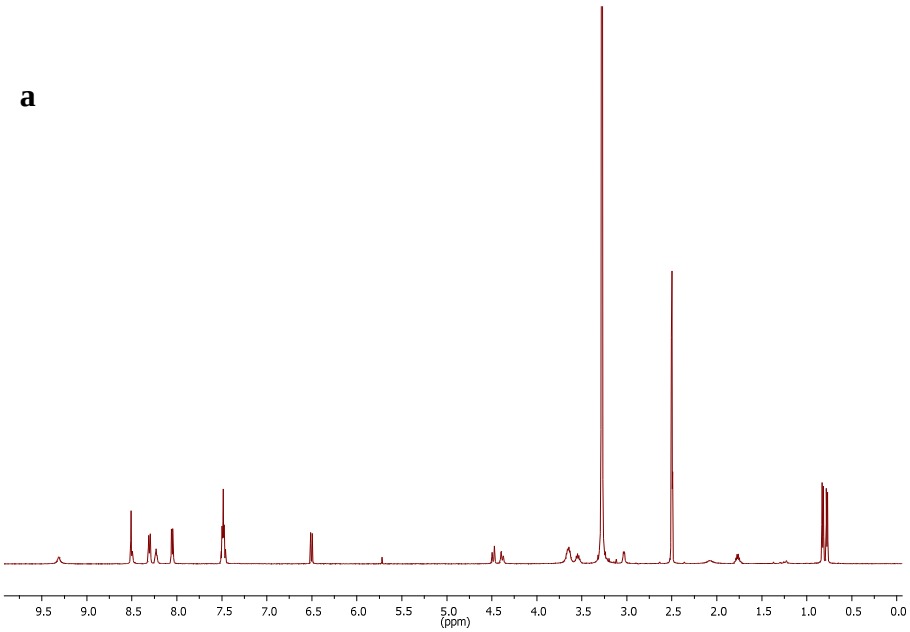

b

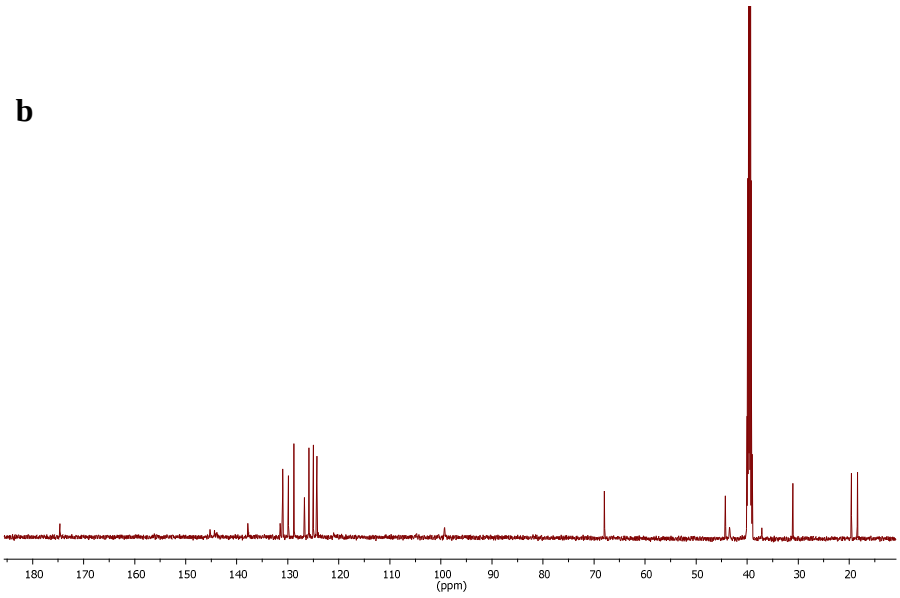

c

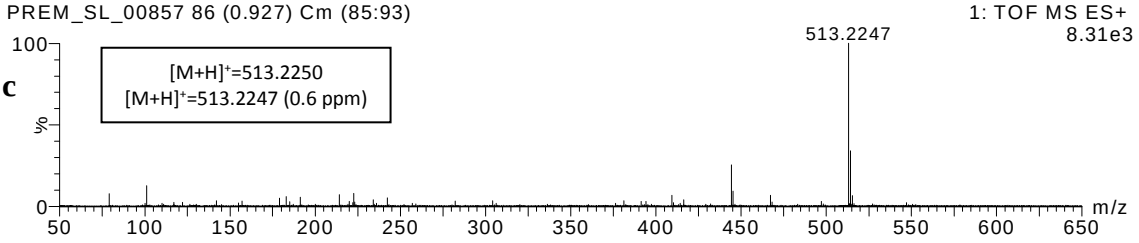

Fig. S2. a) ^{1}H-NMR spectrum in DMSO-d_6, **b)** ^{13}C-NMR spectrum in DMSO-d_6 and **c)** ESI-TOF spectrum of compound **2**.

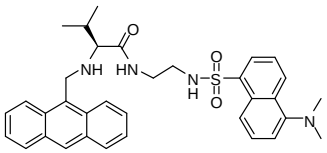

3

a

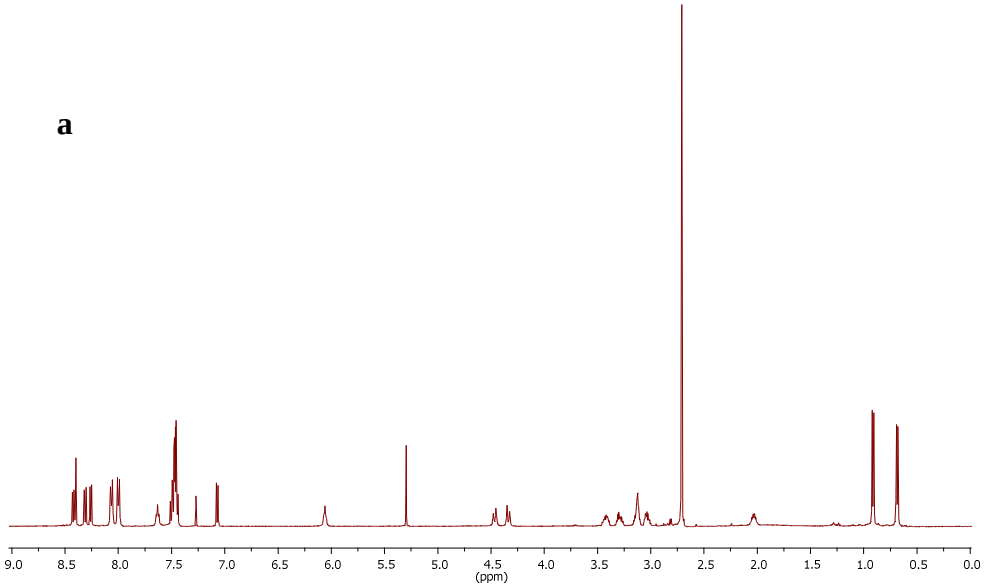

b

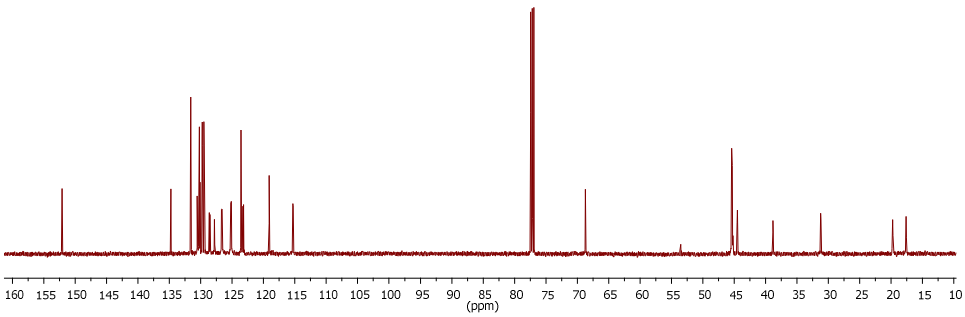

c

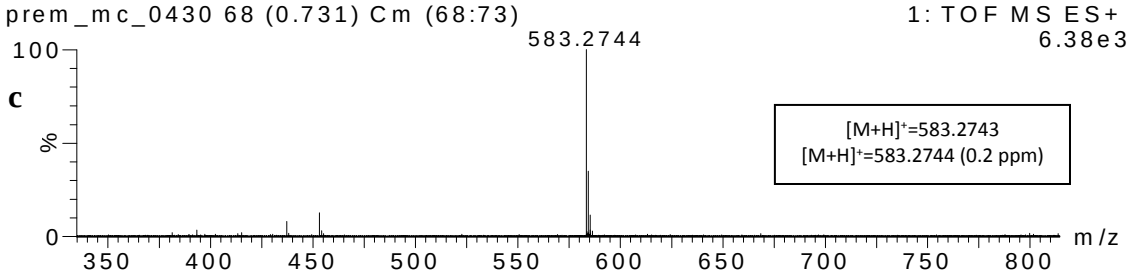

Fig. S3. a) ^{1}H-NMR spectrum in $CHCl_3$-*d*, **b)** ^{13}C-NMR spectrum and in $CHCl_3$-*d* and **c)** ESI-TOF spectrum of compound **3**.

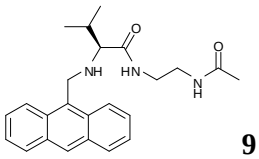

9

a

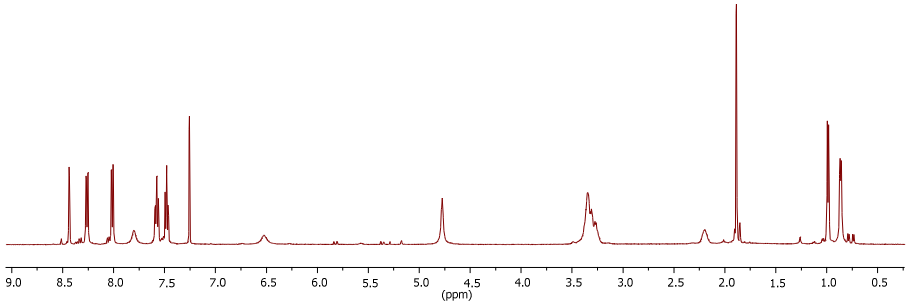

b

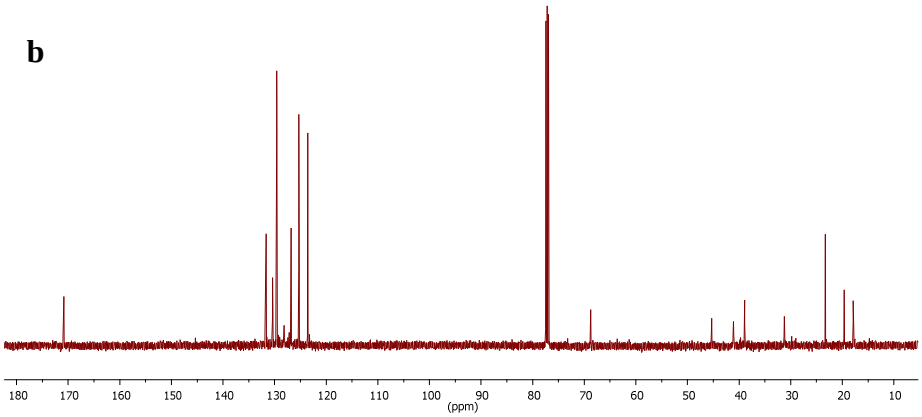

c

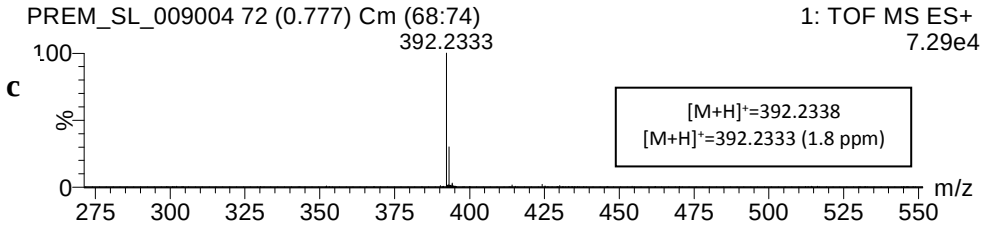

Fig. S4. a) ^{1}H-NMR spectrum in $CHCl_3$-*d*, **b)** ^{13}C-NMR spectrum and in $CHCl_3$-*d* and **c)** ESI-TOF spectrum of the anthracene-acetamide model compound **9**.

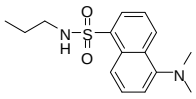

10

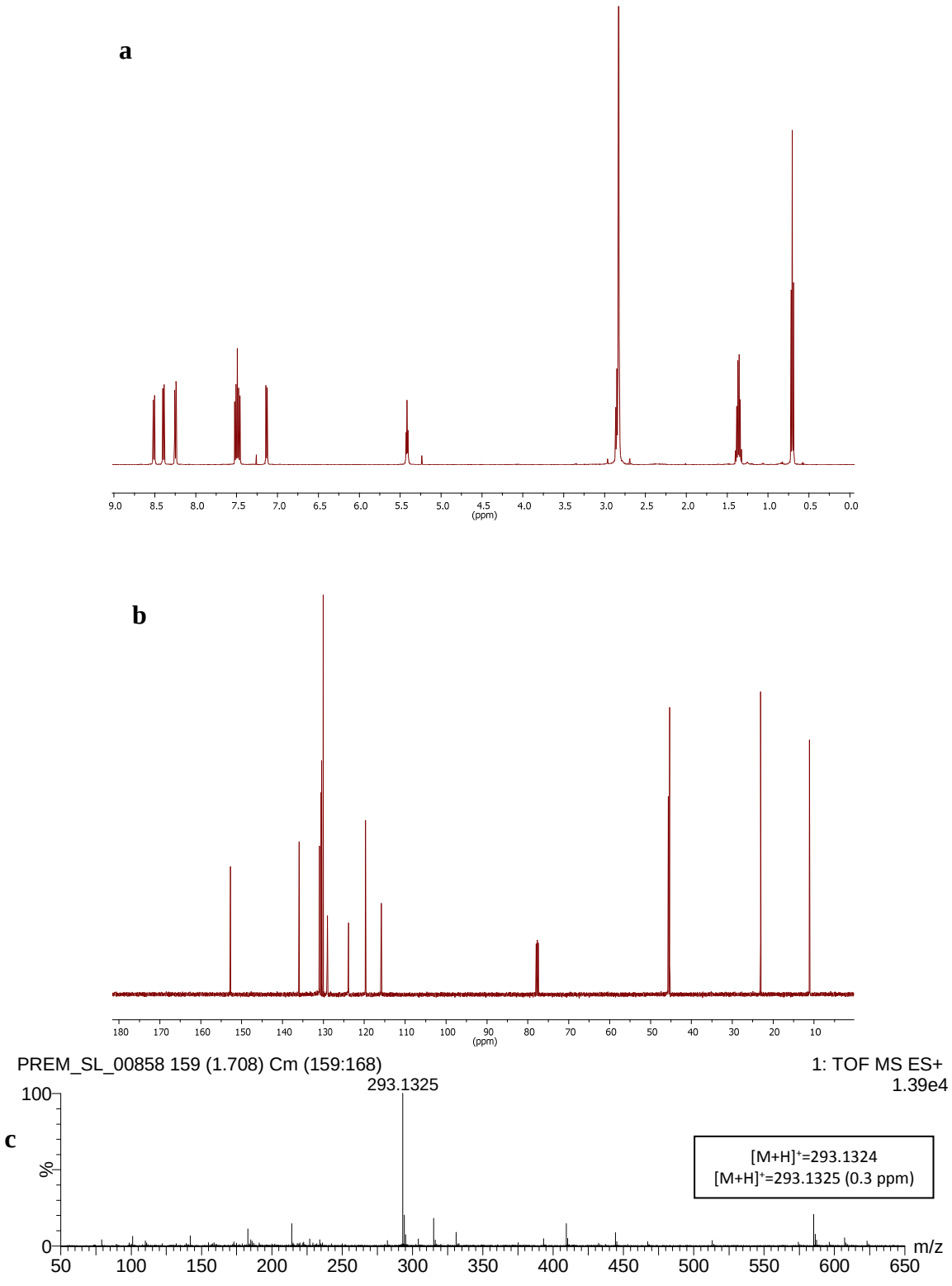

Fig. S5. a) ^{1}H-NMR spectrum in $CHCl_3$-*d*, **b)** ^{13}C-NMR spectrum and $CHCl_3$-*d* and **c)** ESI-TOF spectrum of the dansyl-propyl model compound **10**.

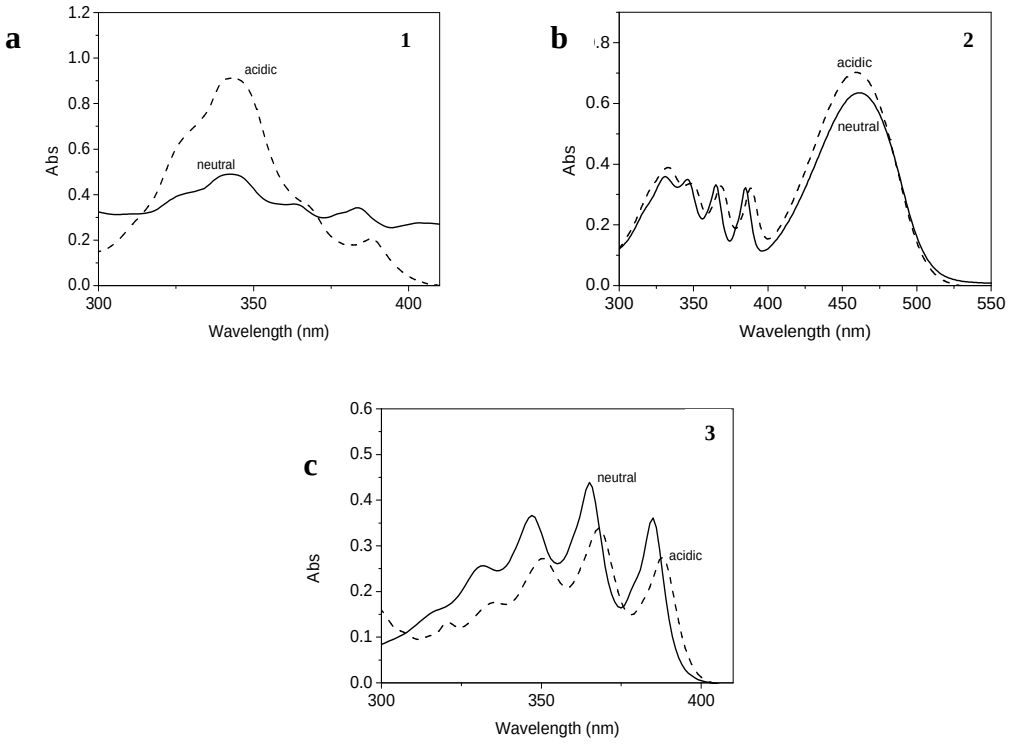

Fig. S6. **a-c)** Absorption spectra of dyads **1-3** ($3.8 \cdot 10^{-5}$ M, $5.3 \cdot 10^{-5}$ M and $3.9 \cdot 10^{-5}$ M, respectively) in MeOH (—) and MeOH with addition of an excess of trifluoroacetic acid (---).

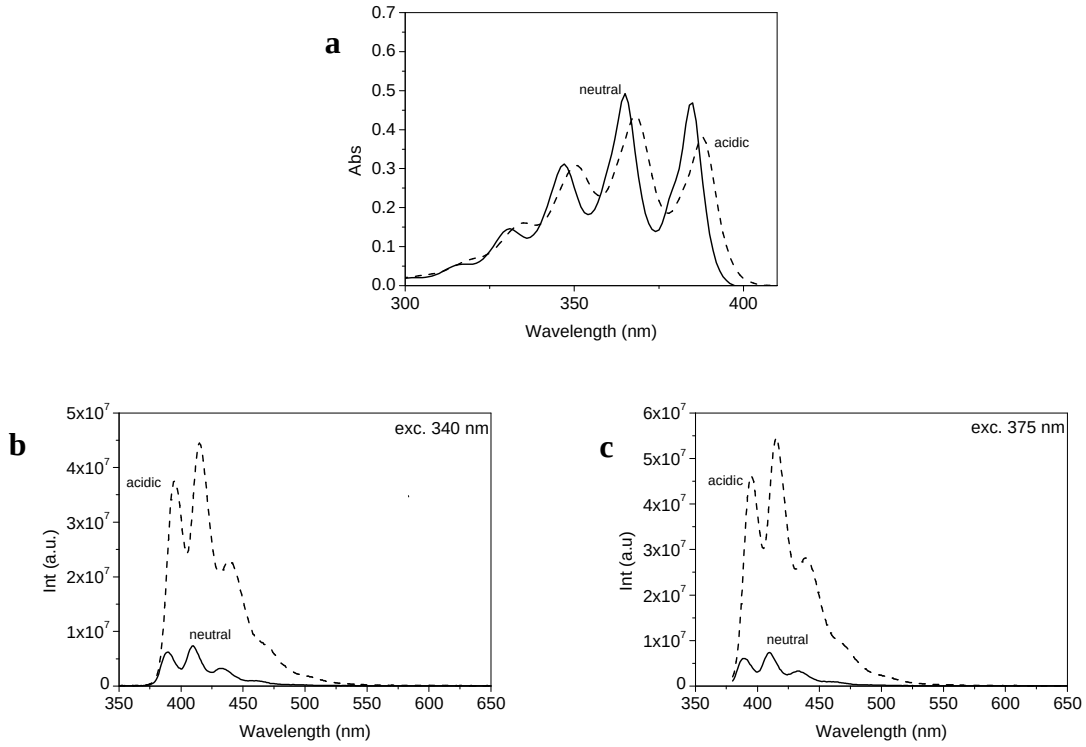

Fig. S7. a) Absorption spectrum, and **b** and **c)** emission spectra of the anthracene-acetamide model compound **9** ($5.56 \cdot 10^{-5}$ M) in MeOH (—) and MeOH with addition of an excess of trifluoroacetic acid (---).

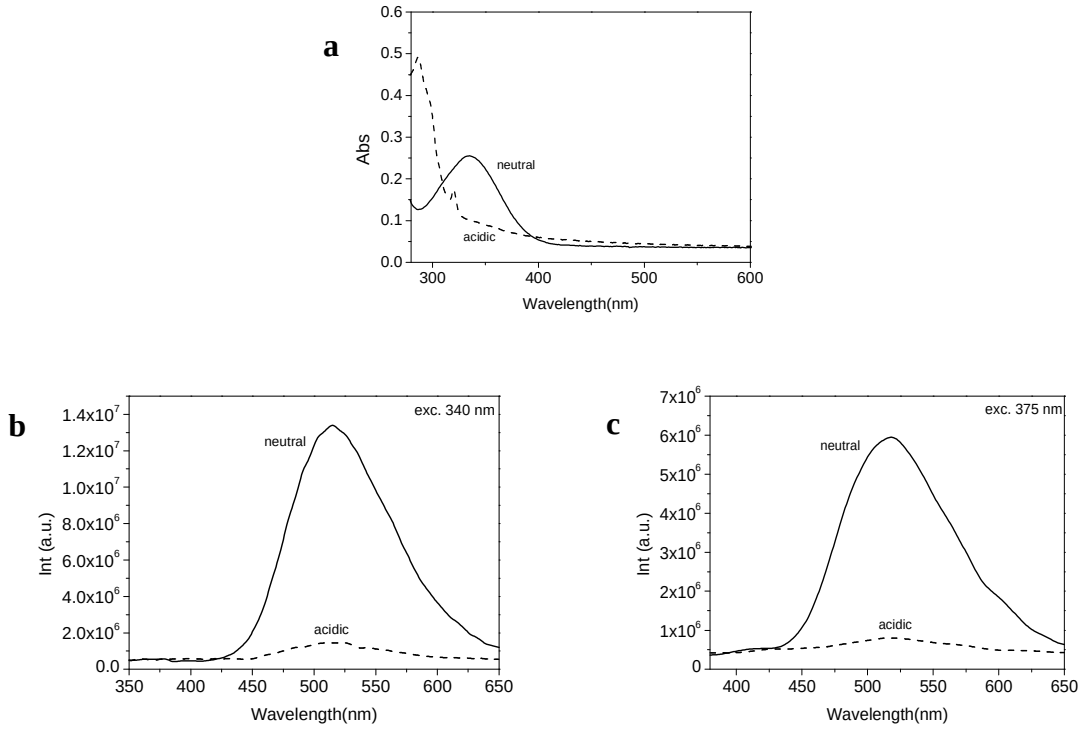

Fig. S8. a) Absorption spectrum, and **b** and **c)** emission spectra of the dansyl-propyl model compound **10** ($5 \cdot 10^{-5}$ M) in MeOH (—) and MeOH with addition of an excess of trifluoroacetic acid (---).

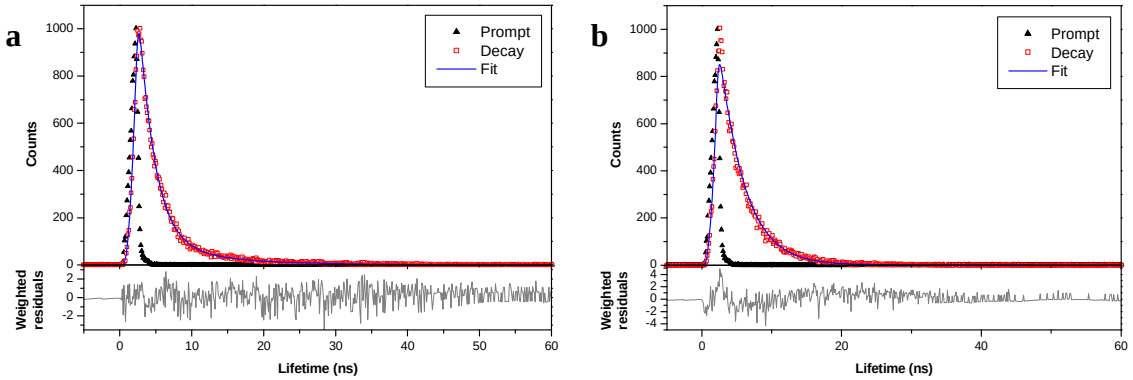

Fig. S9. Fluorescence decay curves of **3** (1.7·10-5 M) in: **a)** MeOH and **b**) MeOH with addition of an excess of trifluoroacetic acid. In neutral media only the emission from the dansyl part was registered, emission from anthracene moiety was too weak to be recorded. In acidic media the emission from the anthracene part was registered, emission from dansyl moiety was too weak to be recorded. λ_{exc}=372 nm. Dansyl moiety life time emission recorded at 550 nm. Anthracene moiety lifetime emission recorded at 420 nm.

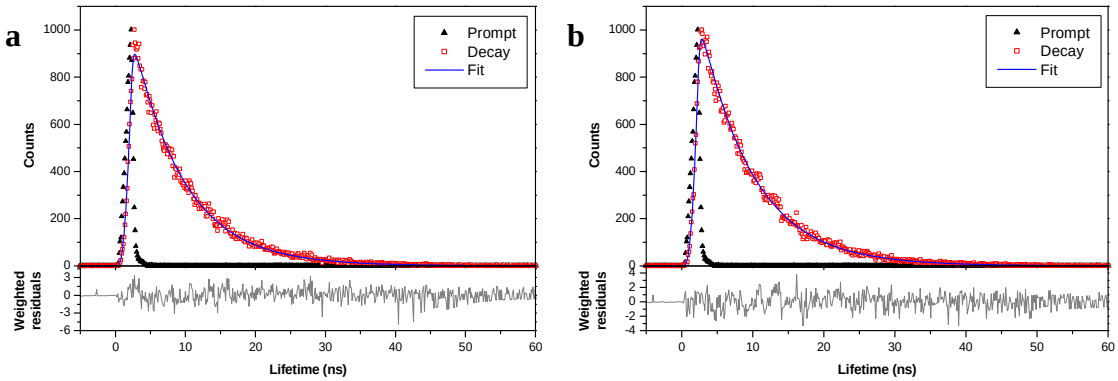

Fig. S10. Fluorescence decay curves of **9** (1.7·10-5 M) in: **a)** MeOH and **b**) MeOH with addition of an excess of trifluoroacetic acid. λ_{exc}=372 nm. Anthracene moiety lifetime emission recorded at 420 nm.

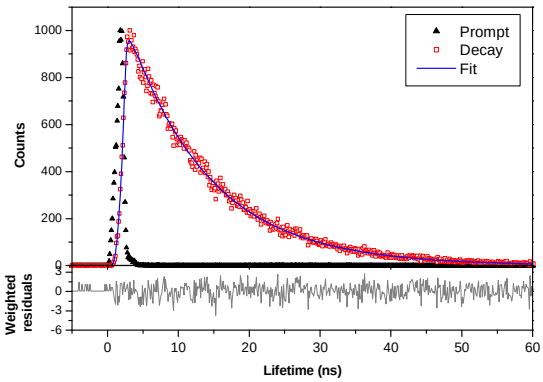

Fig. S11. Fluorescence decay curve of **10** (2.5 10^{-5} M) in MeOH. In acidic media the emission from dansyl moiety was too weak to be recorded. λ_{exc}=372 nm. Dansyl moiety life time emission recorded at 550 nm.

Fluorescence pH titration of the model compounds

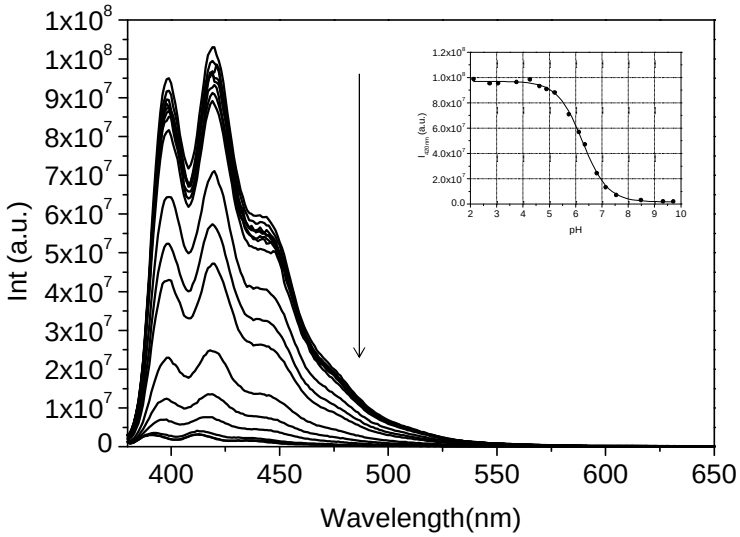

Fig. S12. Fluorescent titration of the anthracene-acetamide model compound **9** as a function of the pH in aqueous solution (1% MeOH). The concentration of the sample was $1 \cdot 10^{-5}$ M. λ_{exc}=375 nm. Inset: pH titration curve of **9**, representation of I_{emis} at 420 nm (fluorescence intensity) *vs.* pH.

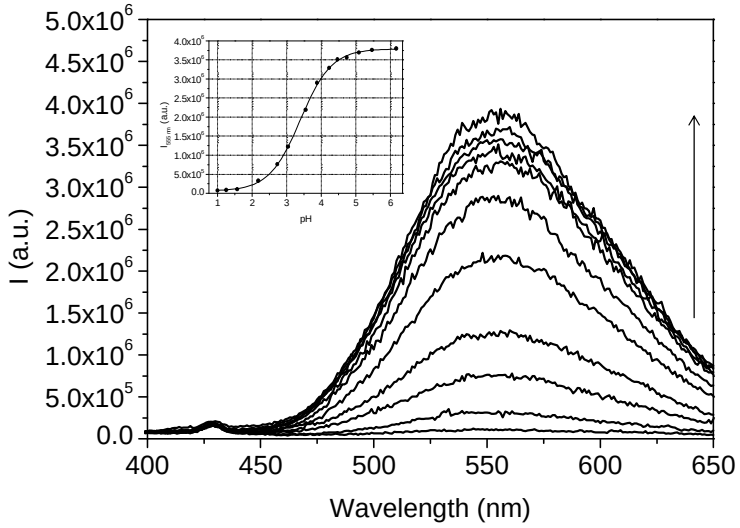

Fig. S13. Fluorescent titration of the dansyl-propyl model compound **10** as a function of the pH in aqueous solution (0.75% DMSO). The concentration of the sample was $7.5 \cdot 10^{-5}$ M. λ_{exc}=375 nm. Inset: pH titration curve of **10**, representation of I_{emis} at 550 nm (fluorescence intensity) *vs.* pH.

NMR Analysis

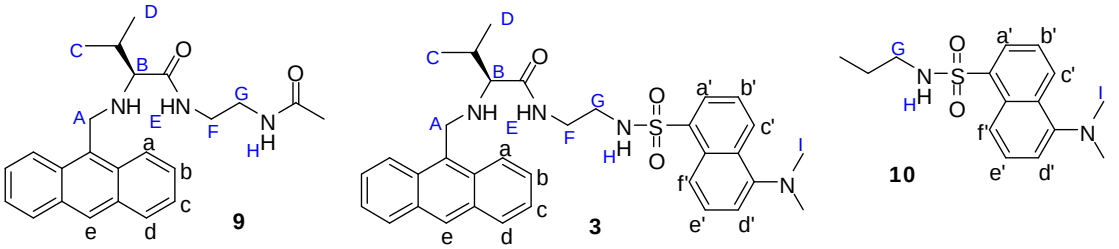

Fig. S14. Signal assignation for NMR interpretation.

Table S1. Analysis of the correlation of the proton signals of the model compounds **9** and **10** with protons of dyad **3** to infer structural information.

Chemical shift (ppm)	9	3	10
a	8.02 (d, *J* = 8.3 Hz, 2H)	7.99 (dd, *J* = 6.2, 3.3 Hz, 2H)	--
b	7.48 (t, *J* = 7.4 Hz, 2H)	7.53 – 7.38 (m, 6H) [+b'+e']	--
c	7.58 (t, *J* = 7.1 Hz, 2H)		--
d	8.26 (d, *J* = 8.8 Hz, 2H)	8.05 (d, *J* = 9.2 Hz, 2H)	--
e	8.44 (s, 1H)	8.39 (s, 1H)	--
A	4.78 (s, 2H)	4.39 (dd, *J*=64.1, 12.5 Hz, 2H)	--
B	3.46–3.21 (m, 5H) [+F+G]	3.50 – 3.35 (m, 1H)	--
C	0.87 (d, *J* = 6.1 Hz, 3H)	0.68 (d, *J* = 6.9 Hz, 3H)	--
D	0.99 (d, *J* = 6.5 Hz, 3H)	0.90 (d, *J* = 6.9 Hz, 3H)	--
E (NH_{amide})	7.80 (bs, 1H)	7.62 (t, *J* = 6.0 Hz, 1H)	--
F	3.46 – 3.21 (m, 5H) [+B]	3.19 – 3.08 (m, 2H)	--
G		3.34 – 3.23 (m, 1H) 3.02 (qd, *J* = 9.2, 4.7 Hz, 1H)	2.90 – 2.79 (m, 8H) [+I]
H($NH_{sulfonamide}$)	6.53 (bs, 1H)	6.05 (t, *J* = 4.9 Hz, 1H)	5.42 (t, *J* = 6.1 Hz, 1H)
I	--	2.70 (s, 6H)	2.90 – 2.79 (m, 8H) [+G]
a'	--	8.30 (d, *J* = 8.6 Hz, 1H)	8.40 (d, *J* = 8.7 Hz, 1H)
b'	--	7.53 – 7.38 (m, 6H) [+b+c+e']	7.53 – 7.45 (m, 2H) [+ e']
c'	--	8.41 (dd, *J* = 8.5, 0.6 Hz, 1H)	8.51 (d, *J* = 8.5 Hz, 1H)
d'	--	7.06 (d, *J* = 7.6 Hz, 1H)	7.13 (d, *J* = 7.5 Hz, 1H)
e'	--	7.53 – 7.38 (m, 6H) [+b+c+b']	7.53 – 7.45 (m, 2H) [+ b']
f'	--	8.25 (d, *J* = 7.3 Hz, 1H)	8.25(dd, *J*=7.3, 1.2 Hz, 1H)

X-ray crystallograpy

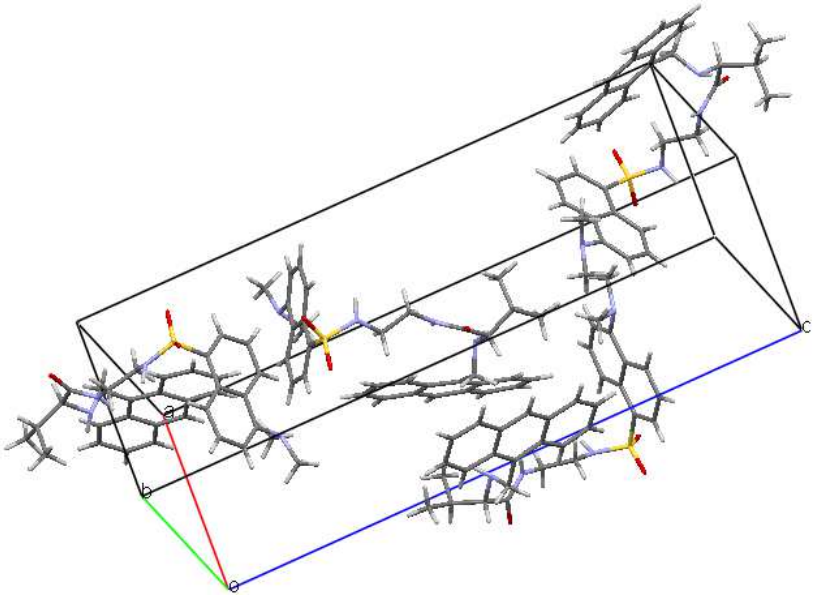

Fig. S15. Crystal cell for **3**.

Table S2. Crystal data and structure refinement for **3**.

Identification code	str1636	
Empirical formula	$C_{34}H_{38}N_4O_3S$	
Formula weight	582.74	
Temperature	293(2) K	
Wavelength	1.54184 Å	
Crystal system	orthorhombic	
Space group	P212121	
Unit cell dimensions	a = 8.7342(2) Å	α= 90°
	b = 12.9336(3) Å	β= 90°
	c = 27.4037(5) Å	γ= 90°
Volume	3095.65(12) $Å^3$	
Z	4	
ρ_{calc}	1.250 g/cm^3	
Absorption coefficient	1.248 mm^{-1}	
F(000)	1240	
Crystal size	0.2286 × 0.2012 × 0.0696 mm^3	
Theta range for data collection	6.46 to 145.16°.	
Index ranges	$-10 \le h \le 9$, $-15 \le k \le 15$, $-33 \le l \le 33$	
Reflections collected	44978	
Independent reflections	6093 [Rint= 0.0261, Rsigma= 0.0123]	
Completeness to theta = 66.97°	99.97 %	

Absorption correction	Gaussian
Refinement method	Full-matrix least-squares on F^2
Data / restraints / parameters	6093/0/391
Goodness-of-fit on F^2	1.039
Final R indices [I≥2σ(I)]	R1 = 0.0312, wR2 = 0.0838
R indices (all data)	R1 = 0.0321, wR2 = 0.0847
Largest diff. peak and hole	0.32 and -0.32e $Å^{-3}$
Absolute structure parameter	0.002(12)
Extinction coefficient	n/a

The X-ray structure obtained for compound **3** is shown in Fig. S16. The presence of an intramolecular hydrogen bond between the hydrogen atom of the amide group and the nitrogen of the amino functionality facilitates a folding of the structure that allows an almost perpendicular arrangement (84º dihedral angle) of the two aromatic rings at a short distance. This intramolecular H-bond is common to many related pseudopeptidic compounds and often defines their final conformational and structural arrangements observed both in the solid state and in solution.[8,9]

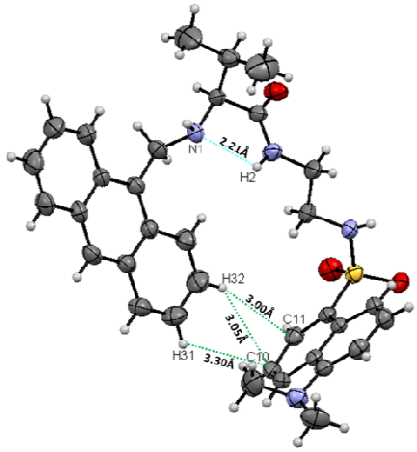

Fig. S16. ORTEP plot of the crystal structure of bichromophoric compound **3** showing an intramolecular H-bond between the hydrogen atom of the amide group and the nitrogen of the amino functionality, which facilitates the occurrence of a folded conformation approaching the two fluorophores, and some of the possible C-H···π interactions between anthracene (CH) and dansyl (π).

An intramolecular offset edge-to-face geometry is adopted by the aromatic rings, with two H-atoms of one of the anthracene rings located at about 3 Å from the closest carbon atoms of the naphthalene from the dansyl moiety. An almost perfect edge-to-edge geometrical disposition is observed, displaying the following parameters: H32···C11 = 3.00 Å, H32···C10= 3.05 Å, H31···C10 = 3.30 Å and H31···C9 = 3.26 Å, representing values of $\%vdW_{H,C}$ of 101.0, 102.7, 111.1 and 109.8, respectively ($\%vdW_{H,C}$ is calculated, for a given measured distance, as the percentage of the sum of the van der Waals radii of H and C:

1.20+1.77 = 2.97 Å).[10] The distance between the centroids of the closest rings is 5.14 Å. It should be noted that a $\%vdW_{H,C}$ value of 100 is by no means the outer limit of an attractive interaction.[11] The $\%vdW_{H,C}$ values obtained for the above mentioned pairs of H-C in structure of **3** are consistent with the range considered by Alvarez for atoms placed at appropriate distances to be likely to establish van de Waals interactions.[10]

The crystal packing (Fig. S17.) involves two columnar antiparallel arrangements of individual molecules associated through a polymeric intermolecular H-bonding network between the sulfonamide hydrogen atoms of a column and the carbonyl oxygen atom of the second one, in such a way that every single molecule of a given column is hydrogen bonded simultaneously to two consecutive molecules of the second column. This arrangement locates the aromatic rings in the outer section, with the anthracene moieties of each column displaying a parallel stacking with a 8.73 Å anthracene-anthracene distance. As corresponds to the antiparallel organization, the planes of the anthracenes in the two columns are not parallel, but tilted by 34.8º. On the contrary, the naphthalene rings of each column are placed almost perpendicular to the anthracene planes and present a parallel displaced disposition with distances of 1.97 Å between the planes defined by the aromatic rings and 6.50 Å between the centroids of the closest rings of the naphthalene moieties, being these centroids displaced in the parallel planes by 6.19 Å, providing a stair-like structure.

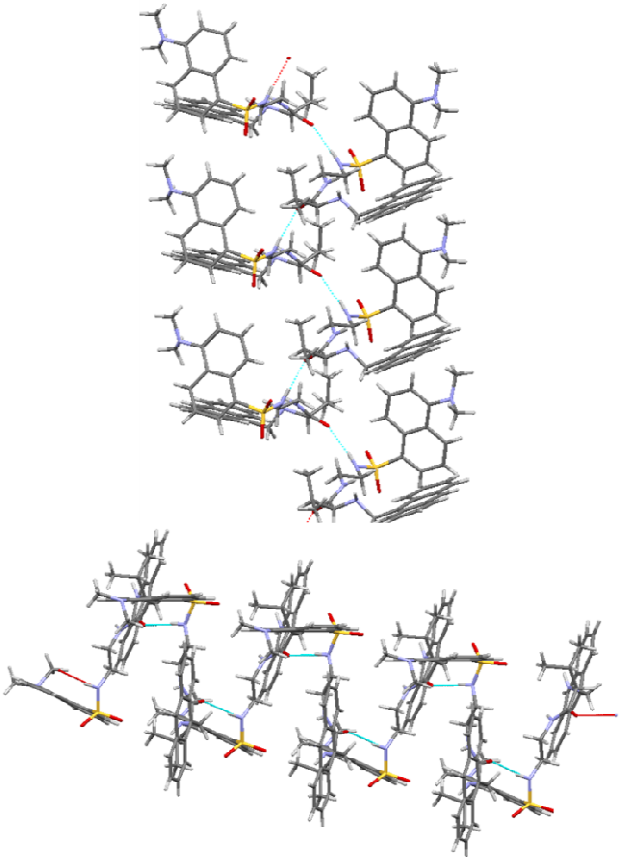

Fig. S17. Crystal packing structure of **3** involving two columnar antiparallel arrangements of individual molecules associated through a polymeric intermolecular H-bonding network.

In the packing structure, each anthracene unit is also located with an intermolecular edge-to-face geometry relative to the naphthalene unit of a third antiparallel column belonging to another pair of antiparallel columns (

Fig. S18.). In this case, the edge of the anthracene ring not involved in the intramolecular edge-to-face geometry is located over the center of the naphthalenic ring bearing the dimethylamino substitution. The closest distances between the corresponding H24 and H25 atoms of the anthracene and the carbon atoms of the naphthalene ring are 3.16 Å (H25-C5) and 3.17 Å (H24-C3), $\%vdW_{H,C}$ *ca.* 106. The angle between the planes defined by both aromatic systems is 71.6º and the distance between the centroids of the involved rings is 5.02 Å. This also locates the anthracene moieties of the two molecules at a relatively short distance, being the distance between the centroids of the central rings 5.48 Å, although the shortest distance between centroids is 5.14 Å. The angle formed between the planes defined by the anthracenes is, as expected from the data obtained from Fig. S17., 34.8º.

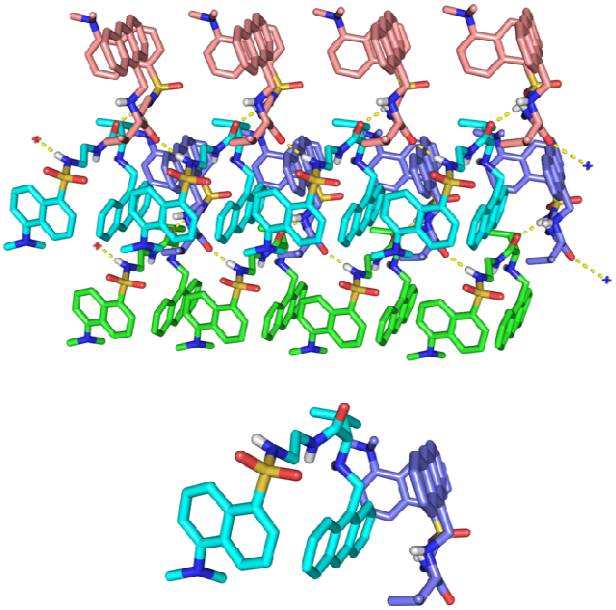

Fig. S18. Packing structure for **3** displaying four rows of columnar arrangements. The expansion shows the relative disposition of two molecules belonging to different rows, showing the close disposition of anthracene and naphthalene units from two different antiparallel arrangements.

Biological studies with live cells

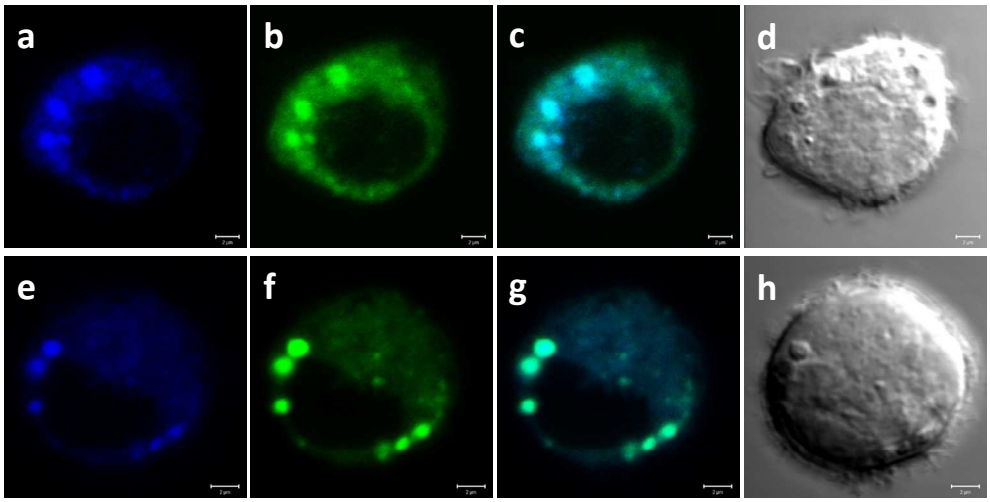

Fig. S19. Confocal fluorescence microscopy images of RAW 264.7 cells loaded with compound **3** for: **a**–**d**) 30 min and **e**-**h**) 5 min. Fluorescence images collected in: **a** and **e)** blue channel (380-430 nm, λ_{exc}=364 nm), **b** and **f)** green channel (470-500 nm, λ_{exc}=364 nm), and **c** and **g)** composite images of blue and green channels. **d** and **h)** Differential interference contrast (DIC) images. Scale bars: 2 µm.

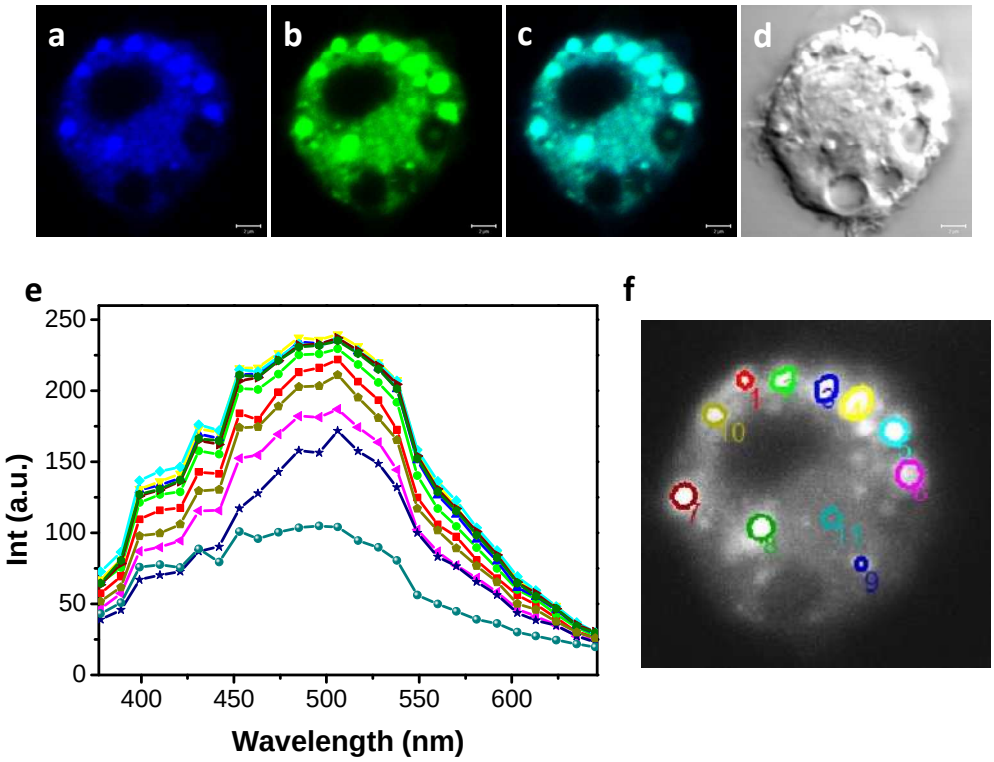

Fig. S20. Confocal fluorescence microscopy images of a RAW 264.7 cell loaded with compound **3**. Fluorescence images collected in: **a)** blue channel (380-430 nm, λ_{exc}=364 nm), **b)** green channel (470-500 nm, λ_{exc}=364 nm), and **c)** composite images of blue and green channels. **d)** Differential interference contrast (DIC) image. Scale bars: 2 µm. **e)** The fluorescence emission spectrum of the selected areas within a RAW 264.7 cell shown in **f)** loaded with compound **3**.

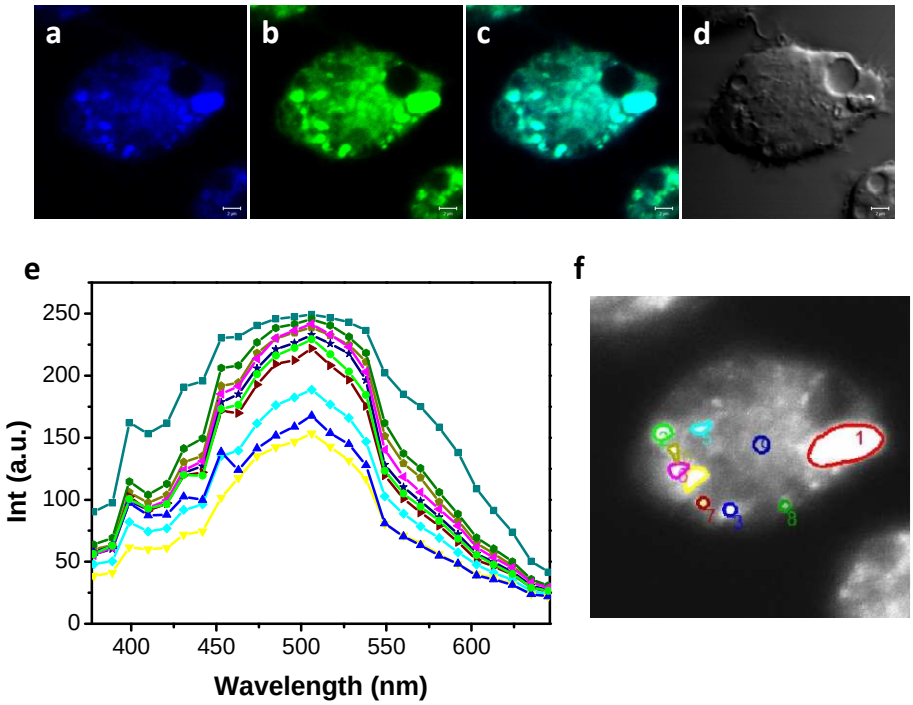

Fig. S21. Confocal fluorescence microscopy images of a RAW 264.7 cell loaded with compound **3**. Fluorescence images collected in: **a)** blue channel (380-430 nm, λ_{exc}=364 nm), **b)** green channel (470-500 nm, λ_{exc}=364 nm), and **c)** composite images of blue and green channels. **d)** Differential interference contrast (DIC) image. Scale bars: 2 µm. **e)** The fluorescence emission spectrum of the selected areas within a RAW 264.7 cell shown in **f)** loaded with compound **3**.

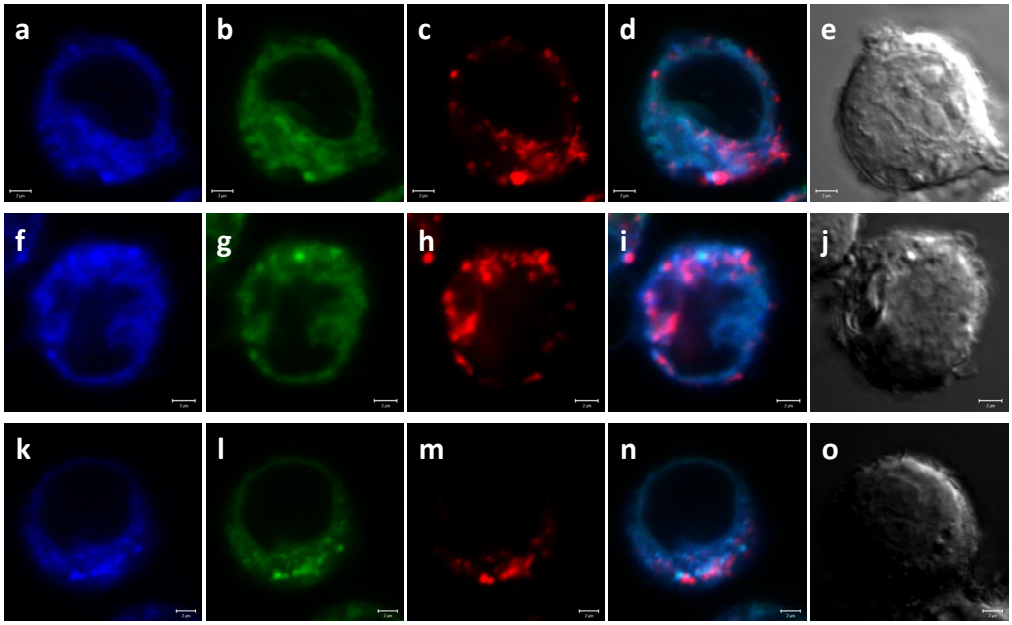

Fig. S22. Confocal fluorescence microscopy images of a RAW 264.7 cells loaded with compound **3** and LysoTracker Red DND-99. Fluorescence images correspond to the fluorescence emission due to: **a**, f and **k)** anthracene chromophore in compound **3** (blue channel, 380-430 nm, λ_{exc}=364 nm), **b**, **g** and **l)** dansyl chromophore in compound **3** (green channel, 470-500 nm, λ_{exc}=364 nm), **c**, **h** and **m)** LysoTracker Red DND-99 (red channel, above 560 nm, λ_{exc}=543 nm), **d**, **i** and **n)** composite images of blue, green and red channels, and **e**, **j** and **o)** DIC images. Scale bars: 2 µm.